Surface Oxide Formation during Rapid Heating of Zn-coated Press Hardening Steel

Chang Wook LEE,[1] Won Seok CHOI,[1] Yeol Rae CHO[2] and Bruno Charles De COOMAN[1]*

1) Graduate Institute of Ferrous Technology, Pohang University of Science and Technology, Pohang, 790-784 South Korea.
2) POSCO Technical Research Laboratories, Gwangyang, 545-090 South Korea.

During the conventional die-quenching processing of a galvanized PHS steel, a thick ZnO layer is formed at the surface. When the heating rate is increased, the oxide at the surface is a thin Al_2O_3 layer. This remarkable change in surface oxide during rapid heating is due to the partial melting of the coating instead of the solidification of the coating and the formation of Fe–Zn intermetallics. In the present study, the characterization of the surface oxide formation at different heating rates is presented.

KEY WORDS: Press Hardening Steel (PHS); galvanized coating; Al_2O_3 layer.

1. Introduction

The need for the development of passenger cars with low fuel consumption is driving the replacement of lower strength automotive steel grades by ultra-high strength steel grades. The use of ultra-high strength steel has been shown to contribute significantly to car body mass containment.[1,2] The most efficient way to produce ultra-high strength auto body parts is the press hardening process as an ultra-high strength steel microstructure is readily obtained by die-quenching. The initial microstructure of press hardening steel (PHS) is a ferrite-pearlite microstructure.[3] The steel is heat treated above 1 173 K (900°C) to obtain a fully austenitic microstructure and simultaneously press formed and die-quenched by water-cooled forming dies to obtain a fully lath martensite microstructure. The ultimate tensile strength is typically above 1.5 GPa and the yield strength is approximately 1 GPa.[4] The high temperature forming significantly reduces the spring back and the tool wear.[1,5] These advantages have resulted in a surge in the use of PHS used for the manufacturing of automotive body anti-intrusion parts and structural reinforcements, such as side impact beams, bumpers, and B pillars.[6–9]

The alloy composition of PHS grades typically contains boron and chromium as hardening agents. These additions retard the ferrite formation during the austenite decomposition.[10] The hardenability of PHS is such that the steel has a lath martensite microstructure when the cooling rate during die-quenching is larger than –25 Ks⁻¹.[11] For lower cooling rates, the microstructure may contain bainite or even ferrite, which causes a decrease in YS and UTS.[12] When an uncoated PHS is used, iron oxide scale is formed during the blank heating causing an unbalanced heat transfer and die surface

damage. The scale is therefore removed by chromium shot blasting, a process which leaves a thin Cr film on the surface. This is beneficial in terms of corrosion resistance.[13] Surface decaburization of uncoated PHS also causes the mechanical properties to be inhomogeneous.[14] Hence, various coating systems have been developed to protect the steel during heating and provide corrosion resistance to the formed parts after the press hardening process. The hot dip Al-10% Si alloy coating is the most widely used coating for press hardening because of its excellent barrier protection. The coating does however not provide cathodic protection, and the corrosion of the underlying steel can occur in areas where the coating layer has been damaged during the die-quenching.[15,16] Zn and Zn-alloy coatings have been developed to address this issue, as Zn and Zn-alloys have the advantage of providing cathodic protection to steel. The use of a Zn coating results in a mild form of liquid metal induced embrittlement (LMIE), characterized by micro-crack formation and the presence of a thick ZnO layer at the surface after die-quenching. LMIE occurs during the high temperature deformation due to the formation of a liquid Fe-saturated Zn phase during the peritectic reaction at 782°C. Above 782°C, the Γ-Fe_3Zn_{10} intermetallic phase is replaced by liquid Zn-rich Fe–Zn alloy, which appears to penetrate the grain boundaries. In the presence of stress, this liquid Fe–Zn alloy penetrates grain boundaries in the steel substrate and the weakened grain boundary cohesion act as an initiation site for the formation of small inter-granular cracks. The forming process should therefore preferably be carried out below the melting temperature of the Γ-Fe_3Zn_{10} intermetallic compound. Alternatively the liquid Zn phase can be eliminated by a longer diffusion annealing process, i.e. by extension of the blank soaking time to protect the steel from LMIE.[17] Micro-cracks occur mainly in the part of the blank exposed to high friction during die quenching. The micro-crack formation can be suppressed by the use of

a lubricant to reduce the coating/die friction.[18]

The presence of a surface layer of ZnO results in an increased electrical resistance which is detrimental to resistance spot welding (RSW). It is therefore common practice to remove the surface oxides prior to RSW.[19] This additional process step reduces the productivity and increases the cost of producing ultra-high strength PHS parts. Various rapid heating techniques are therefore now available to increase the productivity of the die-quenching process such as electrical joule heating,[20] induction heating,[21] contact heating[22] and segmented furnaces with two temperature zones.[23]

In this contribution, the effect of the heating rate on the surface oxide formation was investigated for Zn-coated 22MnB5 PHS. It was found that both the microstructure and the composition of the surface oxide layer showed a pronounced dependence on the heating rate.

2. Experimental

A 22MnB5 (Fe-0.21%C-1.23%Mn-0.002%B, in mass%) PHS grade was prepared by vacuum induction melting (VIM) and the ingots were hot rolled and cold rolled to a final thickness of 1.5 mm. The full-hard cold rolled panels were hot-dip galvanized in a laboratory galvanizing simulator. The temperature of the Zn-0.12 mass% Al hot dip galvanizing bath was kept at 723 K (450°C), and the dipping time was fixed at 5 seconds. The thickness of the Zn coating on the PHS was about 10 μm. The press hardening process was simulated in a multi-purpose annealing simulator which uses electrical resistance heating, which provides flexible heating rates. The specimen temperature was monitored by a K-type thermocouple welded to the center of the samples and in four corners of the specimen. The samples were heated to 1173 K (900°C) using a heating rate of +5 Ks^{-1} and +10 Ks^{-1} and held isothermally for 2 min at this annealing temperature. The specimens were then water quenched to room temperature to obtain a fully martensitic microstructure. The specimens were observed in a ZEISS Ultra 55 Field Emission Scanning Electron Microscopy (FE-SEM) and the samples were analysed by Energy Dispersive Spectroscopy (EDS). Transmission Electron Microscopy (TEM) samples were prepared by the focussed ion beam thinning

method in a FEI QUANTA 3D. The microstructural analysis was carried out in a JEOL JEM-2100F Field Emission Transmission Electron Microscopy (FE-TEM) operated at 200 kV and the samples were analysed by EDS In addition, the surface roughness of the sample was measured with a BMT laser type roughness analyser.

3. Results

Figure 1 shows macro images of the surface of Zn-coated 22MnB5 PHS specimens which were heat treated with the heating rates of +5 Ks^{-1} and +10 Ks^{-1}. The discolouration of the surfaces was significantly different in both cases. The specimen heat treated with a low heating rate had a brown-colored surface whereas the specimen heat treated with a high heating rate had a light grey surface appearance. This striking change in appearance was a first indication that the heating rate had a pronounced influence on the surface oxidation mechanism. The surface roughness of the specimen heat treated with a heating rate of +5 Ks^{-1} was also larger than for the specimen heat treated with a heating rate of +10 Ks^{-1} as shown in the SEM micrograph in Fig. 1. The measured root-mean-square average surface roughness value (R_q) was 2.00 μm for the specimen heat treated with a heating rate of +5 Ks^{-1}. The R_q value of the specimen heat treated with a heating rate of +10 Ks^{-1} was 0.86 μm. In addition, the low magnification image of the surface of the specimen processed with a heating rate of +10 Ks^{-1} had linear features consisting of a mixture of Mn$_3$O$_4$ and ZnO. This local enrichment was absent at the surface of the specimen processed with a heating rate of +5 Ks^{-1}, for which the distribution of Mn$_3$O$_4$ and ZnO was uniform.

Figure 2 shows a bright field (BF) STEM micrograph and the corresponding diffraction patterns of the surface of a specimen heated to 1173 K (900°C) with a heating rate of +5 Ks^{-1}. The surface of the Zn-alloy was covered by a 1–2 μm thick layer comprising three different oxides, which were identified as Mn$_3$O$_4$, ZnO and Al$_2$O$_3$. The selected-area electron diffraction patterns (SADP) of [110]-oriented tetragonal Mn$_3$O$_4$ and [0$\bar{1}$10]-oriented HCP ZnO are shown in Fig. 2. The Al$_2$O$_3$ layer was formed below the thick Mn$_3$O$_4$–ZnO surface oxide layer. This layer did not fully
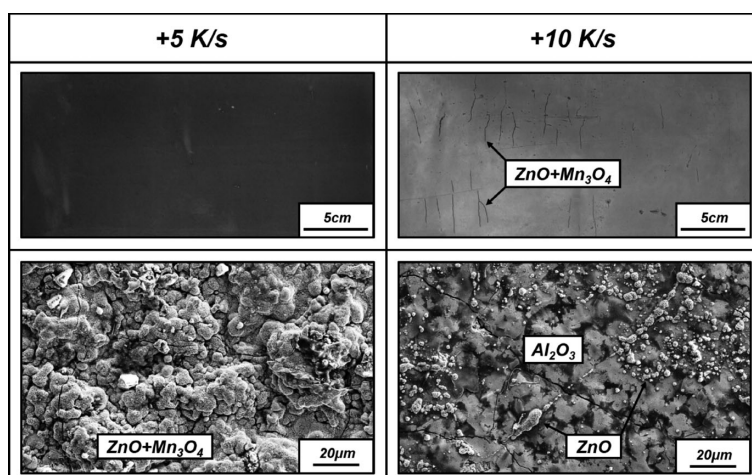

Fig. 1. SEM micrographs of the surface of Zn-coated 22MnB5 PHS specimens heated to 1173 K (900°C) with heating rate of +5 Ks^{-1} and +10 Ks^{-1}.

cover the interface between the Mn_3O_4–ZnO oxide layer and the Fe–Zn alloyed coating layer. A diffraction ring pattern was obtained for the Al_2O_3. There were multiple pores of about 1–2 μm in size between the Mn_3O_4 oxide layer and Fe–Zn alloy coating layer. The Al_2O_3 oxide was not fully attached to coating layer.

Figure 3 shows the dark field (DF) STEM micrograph, the corresponding EDS elemental distribution for Al, Zn,
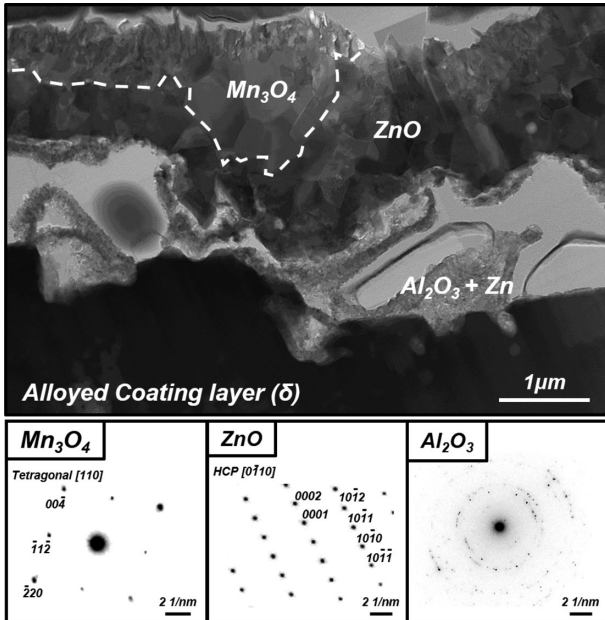
Mn and O, and the chemical composition of specific areas of the specimen shown in Fig. 2. The elemental maps and the compositional line profile confirmed that the topmost oxide layer was composed of two oxide phases, Mn_3O_4 and ZnO. Point 1 in Fig. 3 indicates the presence of Mn_3O_4 (60 wt.% Mn, 20 wt.% O and 19 wt.% Zn). Point 2 in Fig. 3 indicates the presence of ZnO (86 wt.% Zn, 9 wt.% O and 5 wt.% Mn). The coating layer close to surface (Point 4) was identified as the δ-$FeZn_{10}$ intermetallic compound which contain about 10 wt.% of Fe. This intermetallic is very likely liquid at the soaking temperature. The Zn concentration of the topmost surface layer depends on how much Fe has diffused into the coating layer. The Al_2O_3 layer was present at the gaps between the alloyed coating layer and the surface Mn_3O_4–ZnO oxide layer (Point 3).

Figure 4 shows a BF STEM micrograph and the corresponding SADPs of the surface of a specimen heated to 1 173 K (900°C) with a heating rate of +10 Ks^{-1}, and kept at this temperature for 2 min prior to quenching to room temperature. The surface was covered by a continuous thin oxide layer. The thickness of the oxide layer was approximately 200 nm. The SADP of the layer consisted of a ring pattern consistent with the presence of fine-grained Al_2O_3. Some isolated islands of ZnO were present on top of this Al_2O_3 layer. Figure 4 shows the SADP of the ZnO corresponding to the HCP $[01\bar{1}0]$ zone axis. No Mn oxides were observed in the TEM samples. Compared to the specimen heat treated with a heating rate of +5 Ks^{-1}, the Al_2O_3 oxide layer on the surface of the specimen heat treated with a heating rate of +10 Ks^{-1} was compact and covered the entire surface. The elemental distribution confirmed that the continuous surface oxide layer was composed of Al and O. The
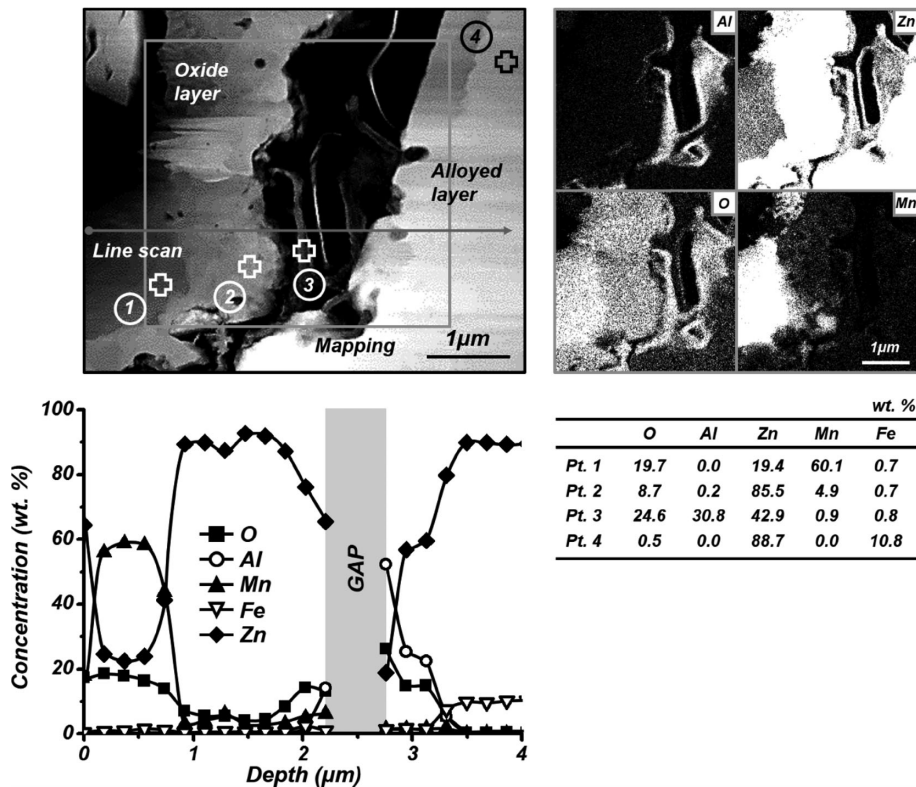

Fig. 2. STEM BF image and SADPs of the surface oxides formed on Zn-coated 22MnB5 PHS heated to 1 173 K (900°C) with a heating rate of +5 Ks^{-1}.

	O	Al	Zn	Mn	Fe
					wt. %
Pt. 1	19.7	0.0	19.4	60.1	0.7
Pt. 2	8.7	0.2	85.5	4.9	0.7
Pt. 3	24.6	30.8	42.9	0.9	0.8
Pt. 4	0.5	0.0	88.7	0.0	10.8

Fig. 3. STEM DF image, elemental distribution of Al, Zn, Mn and O, and chemical composition obtained by EDS of the surface oxides formed on Zn-coated 22MnB5 PHS heated to 1 173 K (900°C) with a heating rate of +5 Ks^{-1}.

EDS analysis of Point 1 in Fig. 4 indicates that the ZnO contained 89 wt.% (67 at.%) Zn and 11 wt.% (32 at.%) O. The δ-FeZn$_{10}$ intermetallic compound was the main constituent of the alloyed coating layer below the Al$_2$O$_3$ layer.

4. Discussion

The mechanism of surface oxide formation for conventional die-quenched PHS was reported by Autengruber et al.[24] They reported that the surface oxide was composed of ZnO and the spinel-type oxide Mn$_3$O$_4$ (Hausmannite). They also reported the presence of Al$_2$O$_3$ fragments under the surface mixture of ZnO and Mn$_3$O$_4$. They argued that the Al$_2$O$_3$ was initially formed as a surface layer and that it prevented oxidation during the heating stage. When the coating was transformed from a liquid phase to Fe–Zn intermetallic compounds, the coating layer solidified and crystallized. This solidification caused the volume of the coating to con-

tract. It resulted in an increased surface roughness and a change of the surface morphology. These processes also damaged the Al$_2$O$_3$ layer, causing the oxidation of Mn and Zn where the Al$_2$O$_3$ layer was damaged. Two phase formations occurred: the δ-FeZn$_{10}$ intermetallic phase was formed at 823 K (550°C) and the formation of the Γ-Fe$_3$Zn$_{10}$ intermetallic phase occurred at 973 K (700°C).[24]

In the case of the rapid heating to the soaking temperature, the surface oxide formation mechanism was clearly different. When the heating rate is low, there is enough time for the formation of the δ and Γ phases. As a consequence the coating is entirely solidified by formation of these Fe–Zn intermetallic compounds. When the heating rate is high however, the coating layer remains partially liquid during the heating, and the top most surface layer is maintained in the liquid state. It therefore remains flat and smooth, allowing for the Al$_2$O$_3$ oxide layer to remain at the surface without being damaged by a change of the topology of the surface. The presence of the thin and continuous Al$_2$O$_3$ surface layer also suppressed further oxidation. This oxide formation mechanism is summarized by the schematics shown in **Fig. 5**.

At the surface of specimens heated to the soaking temperature using a heating rate of +10 Ks^{-1}, line-shaped mixtures of Mn$_3$O$_4$ and ZnO were formed, as shown in Fig. 1. **Figure 6** shows a cross sectional SEM micrograph and an EDS depth profile of a typical line-shaped traces of Mn$_3$O$_4$ and ZnO. The specimen was Ga$^+$-ion milled using a focused ion beam making a 20° angle with the surface. The sample was tilted 70° to allow for chemical analysis of the ion-milled cross-section by EDS. The Mn$_3$O$_4$–ZnO oxide trace was approximately 20 μm wide.

Mn containing particles were also observed in the Zn-rich areas which were liquid at 1 173 K (900°C). The presence of Mn in the coating is due to the fact that the Mn from the steel substrate is soluble in the liquid Zn bath during the galvanizing process, and that galvanizing baths are typically Mn-saturated, in addition to being Fe-saturated. The Mn oxide at the surface of the coating layer is due to the oxidation of the Mn present in solution in the molten Zn bath. An additional source of Mn is due to the interdiffusion of the substrate into the coating.[25] The oxidation was clearly initiated where crevices in the Al$_2$O$_3$ layer were formed. The oxides were large because the oxidation was concentrated at these areas. The presence of these oxides can in principle be avoided by controlling the purity of the Zn bath although
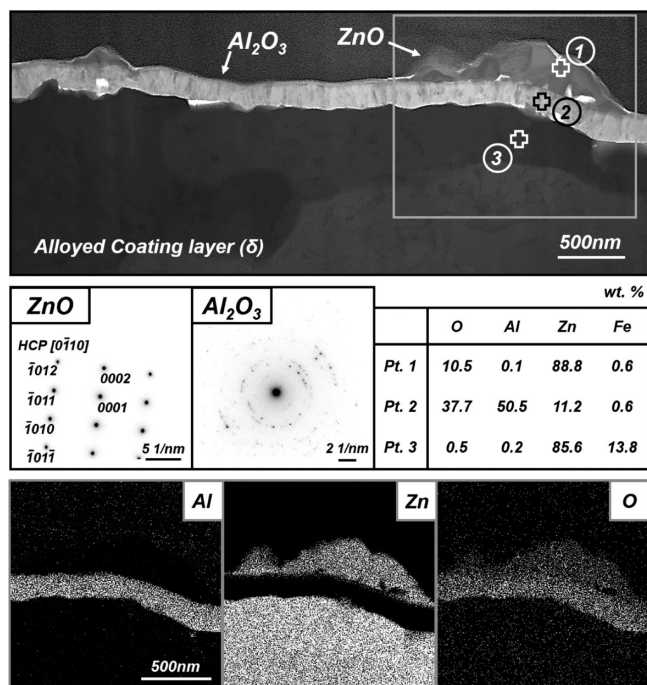
Fig. 4. STEM BF micrograph and corresponding SADPs, elemental distribution for Al, Zn and O, and chemical composition of specific areas as obtained by EDS for the surface oxide on Zn-coated 22MnB5 PHS heated to 1 173 K (900°C) with a heating rate of +10 Ks^{-1}.
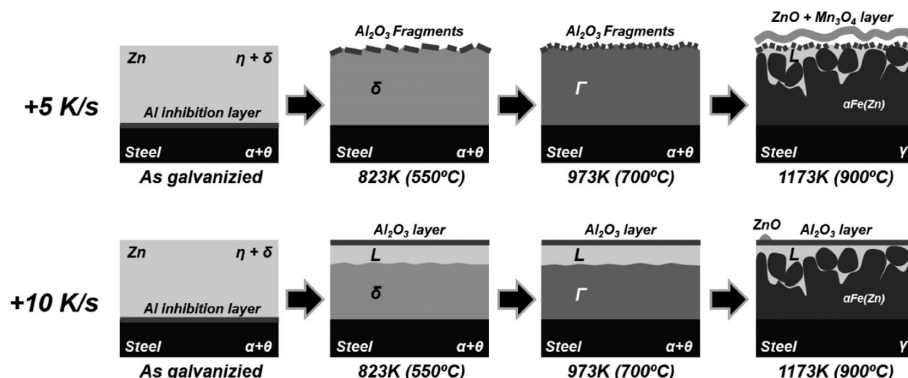
Fig. 5. Schematic of oxide formation mechanisms during conventional heating (+5 Ks^{-1}) and rapid heating (+10 Ks^{-1}).
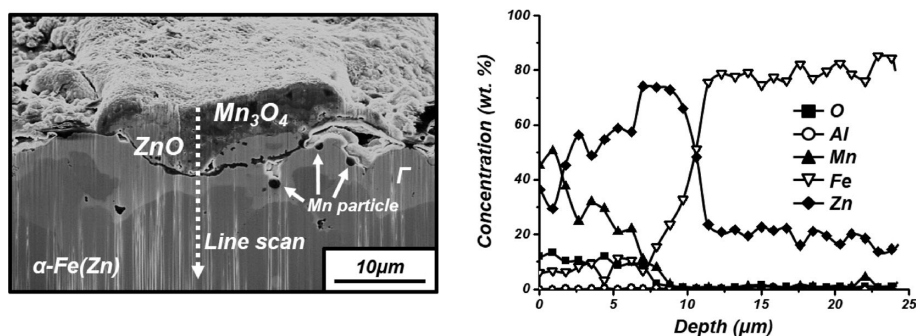
Fig. 6. SEM cross-sectional micrograph and EDS elemental depth profiles of the line-shaped Mn_3O_4–ZnO oxide mixture formed at the surface of Zn-coated 22MnB5 PHS heated to 1 173 K (900°C) with a heating rate of +10 Ks^{-1}.

galvanizing baths are usually saturated with the major steel alloying elements in steel such as Mn, which is an ubiquitous alloying addition in steel.

The surface oxidation of a Zn-coated PHS during a die-quenching process with a high heating rate is expected to provide two major benefits. First, the resistance spot welding characteristic of the PHS parts will be improved. The presence of a gap between the alloyed coating layer and the oxide layer as observed in samples after a slow heating to the soaking temperature, reduces the confinement of the molten zone during the welding process and increases the likelihood of weld metal expulsion and a reduction of the welding current range. Faderl *et al.* reported that dry-ice cleaning of Zn-coated PHS surface can improve the weldability.[19] This additional process will however affect the productivity and impact the production cost negatively. The rapid heating discussed in the present contribution offers a more effective alternative. Although the weldability has not yet been analysed, it is expected that it will be improved due to the excellent adhesion between the thin Al_2O_3 surface layer and alloyed coating layer. No additional process for the removal of the ZnO is required. The micro-crack problem is also expected to be less pronounced. Drillet *et al.* reported that micro-cracks propagate along martensite/ferrite interfaces. The formation of this crack propagation path can be suppressed by increasing the cooling rate or by using a lubricant.[18] The rapidly heated PHS had a very smooth surface profile as shown in Fig. 1. This smoother surface is expected to result a lower friction during press forming. The formation of surface asperities during conventional heating with a lower heating rate, acts to increase the friction during forming. The rapid heating to the soaking temperature is therefore expected to be beneficial for suppressing micro-crack formation during die-quenching of Zn coated PHS.

4. Conclusion

Rapid heating to the soaking temperature of Zn coated PHS resulted in the formation of a thin Al_2O_3 surface layer on a smooth alloyed coating surface. During a conventional heat cycle with a lower heating rate, the Al_2O_3 oxide layer was damaged by the formation of Fe–Zn intermetallic compounds which resulted in the formation of ZnO and Mn_3O_4 above the damaged Al_2O_3 layer. In contrast, the Al_2O_3 oxide layer was not damaged by the formation of Fe–Zn intermetallic compounds during a rapid heating to the soaking temperature.

REFERENCES

1) P. Åkerström: Doctoral Theses, Luleå University of Technology, Sweden, (2006).
2) H. Karbasian and A. E. Tekkaya: *J. Mater. Process. Technol.*, **210** (2010), No. 15, 2103.
3) D. W. Fan, H. S. Kim and B. C. De Cooman: *Steel Res. Int.*, **80** (2009), No. 3, 241.
4) H. Liu, X. Jin, H. Dong and J. Shi: *Mater. Charact.*, **62** (2011), 223.
5) M. Pfesdorf and T. Laumann: Proc. of 3rd Erlanger Workshop Warmblechumformung, (2008), 23.
6) K. Steinhoff, N. Barbakadze and M. Schupfer: Galvatech 2011 Conf., AIM, Genova, (2011), 319.
7) J. Aspacher: 1st Int. Conf. on Hot Sheet Metal Forming of High performance Steel, CHS^2, Kassel, (2008), 268.
8) K. Steinhoff: 1st Int. Seminar on Hot Sheet Metal Frming of High performance Steel, CHS^2, Hanover, (2010).
9) M. Schupfer and K. Steinhoff: 3rd Int. Conf. on Hot Sheet Metal Forming of High Performance Steel, CHS^2, Kassel, (2011), 271.
10) B. C. De Cooman and J. G. Speer: Fundamentals of Steel Product Physical Metallurgy, 1st ed., AIST, Warrendale, PA, (2011).
11) L. Garcia Aranda, Y. Chastel, P. Fernandez, J. Pascual and T. Dal Negro: *Adv. Technol. Plasticity*, **2** (2002), 1135.
12) A. Bardelcik, M. J. Worswick and M. A. Wells: *Mater. Design*, **55** (2014), 509.
13) Steel Bumper Systems for Passenger Cars and Light Trucks, American Iron and Steel Institute, Southfield, Michigan, (2003).
14) W. S. Choi and B. C. De Cooman: *Steel Res. Int.*, **84** (2014), 1.
15) L. Dosdat, J. Petitjean, T. Vietoris and O. Clauzeau: *Steel Res. Int.*, **82** (2011), 726.
16) D. W. Fan, H. S. Kim, J. K. Oh, K. G. Chin and B. C. De Cooman: *ISIJ Int.*, **50** (2010), 561.
17) C. W. Lee, D. W. Fan, I. R. Sohn, S. J. Lee and B. C. De Cooman: *Metall. Mater. Trans. A*, **43** (2012), 5122.
18) P. Drillet, R. Grigorieva, G. Leuillier and T. Vietoris: Galvatech 2011 Conf., AIM, Genova, (2011), 371.
19) J. Faderl: 2nd Int. Conf. on Hot Sheet Metal Forming of High performance Steel, CHS^2, Luleå, (2009), 283.
20) K. Mori, S. Maki and Y. Tanaka: *CIRP Ann-Manuf. Technol.*, **54** (2005), No. 1, 209.
21) R. Kolleck, R. Veit, M. Merklein, J. Lechler and M. Geiger: *CIRP Ann-Manuf. Technol.*, **58** (2009), No. 1, 275.
22) V. Ploshikhin, A. Prihodovsky, J. Kaiser and U. Bach: WO2010048950, (2010).
23) H. Lehmann: 3rd Int. Conf. on Hot Sheet Metal Forming of High performance Steel, CHS^2, Kassel, (2011), 171.
24) R. Autengruber, G. Luckeneder, A. S. Kolnberger, J. Federl and A. W. Hassel: *Steel Res. Int.*, **83** (2012), No. 11, 1005.
25) M. Dubois: Zinc-based Steel Coating System: Production and Performance, TMS, San Antonio, Texas, (1998), 39.